Rules and mechanisms governing octahedral tilts in perovskites under pressure

H. J. Xiang,[1,2,3,*] Mael Guennou,[4] Jorge Íñiguez,[4] Jens Kreisel,[4,5] and L. Bellaiche[2,†]

[1]*Key Laboratory of Computational Physical Sciences (Ministry of Education), State Key Laboratory of Surface Physics, and Department of Physics, Fudan University, Shanghai 200433, P. R. China*

[2]*Physics Department and Institute for Nanoscience and Engineering, University of Arkansas, Fayetteville, Arkansas 72701, USA*

[3]*Collaborative Innovation Center of Advanced Microstructures, Nanjing 210093, P. R. China*

[4]*Materials Research and Technology Department, Luxembourg Institute of Science and Technology (LIST), 41 Rue du Brill, L-4422 Belvaux, Luxembourg*

[5]*Physics and Materials Science Research Unit, University of Luxembourg, 41 Rue du Brill, L-4422 Belvaux, Luxembourg*

(Received 19 February 2017; revised manuscript received 1 May 2017; published 2 August 2017)

The rotation of octahedra (octahedral tilting) is common in ABO_3 perovskites and relevant to many physical phenomena, ranging from electronic and magnetic properties, metal-insulator transitions to improper ferroelectricity. Hydrostatic pressure is an efficient way to tune and control octahedral tiltings. However, the pressure behavior of such tiltings can dramatically differ from one material to another, with the origins of such differences remaining controversial. In this paper, we discover several new mechanisms and formulate a set of simple rules that allow us to understand how pressure affects oxygen octahedral tiltings via the use and analysis of first-principles results for a variety of compounds. Besides the known A-O interactions, we reveal that the interactions between specific B ions and oxygen ions contribute to the tilting instability. We explain the previously reported trend that the derivative of the oxygen octahedral tilting with respect to pressure (dR/dP) usually decreases with both the tolerance factor and the ionization state of the A ion by illustrating the key role of A-O interactions and their change under pressure. Furthermore, three new mechanisms/rules are discovered, namely that (i) the octahedral rotations in ABO_3 perovskites with empty low-lying d states on the B site are greatly enhanced by pressure, in order to lower the electronic kinetic energy; (ii) dR/dP is enhanced when the system possesses weak tilt instabilities, and (iii) for the most common phase exhibited by perovskites—the orthorhombic *Pbnm* state—the in-phase and antiphase octahedral rotations are not automatically both suppressed or both enhanced by the application of pressure because of a trilinear coupling between these two rotation types and an antipolar mode involving the A ions. We further predict that the polarization associated with the so-called hybrid improper ferroelectricity could be manipulated by hydrostatic pressure by indirectly controlling the amplitude of octahedral rotations.

DOI: 10.1103/PhysRevB.96.054102

I. INTRODUCTION

The perovskite structure is one of the most commonly occurring and important structural types in materials science. From both theoretical and applied points of view, perovskite materials are interesting since they display many diverse and intriguing properties, including superconductivity [1], colossal magnetoresistance [2], ferroelectricity [3], multiferroicity [4–6], or photovoltaicity [7]. The ideal perovskite oxide ABO_3 structure adopts the cubic space group $Pm\bar{3}m$, with the A cation surrounded by 12 oxygen anions in a dodecahedral environment and the B cation octahedrally coordinated with six oxygen ions. The perovskite structure can be viewed as a three-dimensional cubic network of corner-sharing BO_6 octahedra with the A cation sitting in the center of a cube defined by eight corner-sharing octahedral units. Although the ideal perovskite structure is cubic, most perovskite oxides are in fact distorted [8]. The most common type of distortion is octahedral rotation, i.e. rigid BO_6 octahedra tilts while maintaining their corner-sharing connectivity [9]. The octahedral rotation, which was believed to be due to the tendency to maximize the number of short A-O interactions [10], can have important effects on physical properties of perovskite compounds, particularly electrical and magnetic [11].

The effect of hydrostatic pressure on properties of perovskites has been investigated for a long time in condensed matter physics, solid state chemistry, materials science, and earth science. For example, an external pressure causes the polar distortion of multiferroic $TbMnO_3$ to flop and leads to the largest polarization values ever reported among spin-driven ferroelectrics [12]. It was also reported that hydrostatic pressure can significantly influence octahedral tilt angles. Regarding the pressure effect on octahedral tiltings, Samara *et al.* [13] proposed in 1975 a rule in terms of the competition between the short-range Pauli repulsion and long-range Coulomb interactions. According to this picture, in the case of zone-boundary distortions (e.g., octahedral tiltings), the short-range interactions would increase with pressure much more rapidly than the long-range couplings, which should result in an increase of octahedral tiltings under pressure. This rule is in agreement with the pressure behaviors in orthorhombic $CaSnO_3$ [14] and $CaTiO_3$ [15] and tetragonal $SrTiO_3$ [16]. However, this rule is violated by experimental results of other materials: For example, rhombohedral $LaAlO_3$ [17], as well as orthorhombic $YAlO_3$,$GdFeO_3$,$GdAlO_3$ [18,19], and $SmFeO_3$ [20], all become less distorted under pressure. Note that the behavior in $LaAlO_3$ was confirmed in a first-principles study [21]. Later on, another empirical rule [22] based on the relative

*hxiang@fudan.edu.cn
†laurent@uark.edu

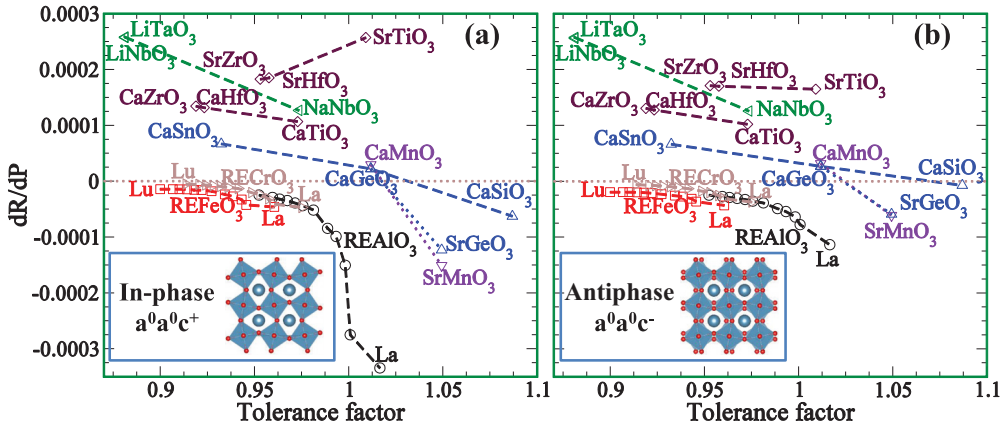

FIG. 1. Derivative of (a) in-phase and (b) antiphase rotation with respect to pressure as a function of the tolerance factor. The results of several series (REFeO$_3$, REAlO$_3$, RECrO$_3$, CaBO$_3$, SrBO$_3$, LiBO$_3$, and NaNbO$_3$) are shown.

compressibility of the AO_{12} and BO_6 polyhedra was proposed to account for the observed differences in behavior among various compounds. This rule states that, for perovskites in which the A cation has a lower formal charge than the B cation (e.g., MgSiO$_3$, CaSnO$_3$, or CaSiO$_3$), the AO_{12} polyhedra are more compressible than the BO_6 octahedra, and as a result, the tilts of the BO_6 octahedra increase with pressure, thereby reducing the unit-cell volume. In contrast, whenever the A and B cations have the same formal charge (e.g., LaAlO$_3$ and GdFeO$_3$), the BO_6 octahedra are more compressible than the AO_{12} polyhedra, and as a consequence, the tilts of the octahedra decrease with increasing pressure, thus evolving towards the cubic phase. However, the rule of Angel *et al.* [22] is in conflict with (i) a density functional study predicting that pressure gradually reduces (rather than enhances) the tilting of the SiO$_6$ octahedra in orthorhombic CaSiO$_3$ [23]; (ii) first-principles calculations showing that the instability of antiphase tiltings becomes stronger (rather than weaker) with increasing pressure for the cubic phase of REAlO$_3$ compounds with small rare-earth (RE) ions (e.g., Er) [21]; and (iii) a recent Raman scattering and synchrotron powder x-ray diffraction study suggesting that the octahedral tilts may increase with pressure in RE chromites RECrO$_3$ with small RE ions [24]. Note that the possible failure of this rule was also pointed out by Zhao *et al.* [25]. Therefore, the origin of the distinct pressure behaviors of octahedral tilting in perovskites remains puzzling.

In this paper, we aim at revealing and understanding the origin of the diverse pressure behaviors of octahedral tilting in perovskites by conducting and analyzing first-principles calculations on many different and representative materials. We also report rules/effects pertaining to the effect of pressure on octahedral tilting. Not only does our paper provide a unified set of rules on the effects of pressure, but it also suggests ways to tune these tiltings and, therefore, the properties of perovskites.

II. RESULTS

As indicated in the Appendix, we perform density functional theory (DFT) simulations on a variety of perovskites under hydrostatic pressure.

A. General trends for in-phase and antiphase tiltings

In order to understand the various effects that pressure can have on octahedral tiltings, we first focus on cases for which there is only a single type of tilting about a single pseudocubic axis. In other words, we consider two possibilities: an in-phase tilt about the pseudocubic [001] direction (i.e., $a^0a^0c^+$ in Glazer's notation [9]) and an antiphase tilt about the same axis (i.e., $a^0a^0c^-$). Figure 1 reports our results for the derivative of in-phase and antiphase tilting amplitude with respect to pressure (that is, $dR_{\rm in}/dP$ and $dR_{\rm anti}/dP$, respectively) as a function of the tolerance factor, for many different perovskite materials. Note that the tolerance factor [26] is defined as $t = \frac{r_A + r_O}{\sqrt{2}(r_B + r_O)}$ (where r_A, r_B, r_O denote the radii [27] of the A cation, B cation, and O anion, respectively) and is widely used to discuss the stability of perovskite structures. Here, we consider (i) the REAlO$_3$, REFeO$_3$, and RECrO$_3$ families as representative of $A^{3+}B^{3+}O_3^{2-}$ materials; (ii) the CaBO$_3$ (with B = Ti,Zr,Hf,Si,Ge,Sn,Mn) and SrBO$_3$ (B = Ti,Ge,Mn,Zr,Hf) families as examples of $A^{2+}B^{4+}O_3^{2-}$ compounds; and (iii) LiNbO$_3$, LiTaO$_3$, and NaNbO$_3$ for $A^{1+}B^{5+}O_3^{2-}$ systems (we include LiNbO$_3$ and LiTaO$_3$ here merely for the comparison with NaNbO$_3$). Note that these materials are considered in idealized $a^0a^0c^+$ and $a^0a^0c^-$ structures so that we can investigate general trends in the pressure behavior of an individual tilting pattern, although most of them present more complicated tilting structures in reality.

As shown in Figs. 1(a) and 1(b), the pressure behavior of in-phase tilts is rather similar to that of the antiphase tilts in all considered compounds. We will thus mainly discuss the antiphase case, as this pattern is the most common one among perovskites.

We find that, usually, $dR_{\rm anti}/dP$ decreases with the tolerance factor for each series. For example, for REFeO$_3$, $dR_{\rm anti}/dP$ decreases from -2.0×10^{-5} to -4.3×10^{-5} kbar^{-1} [28] where RE varies from Lu to La. Another interesting trend is that $dR_{\rm anti}/dP$ for the $A^{2+}B^{4+}O_3^{2-}$ and $A^{1+}B^{5+}O_3^{2-}$ families is larger than that for the $A^{3+}B^{3+}O_3^{2-}$ materials. In fact, $dR_{\rm anti}/dP$ is negative for all REAlO$_3$ and REFeO$_3$ compounds, i.e., pressure suppresses the antiphase octahedral tilting in these cases. In contrast, $dR_{\rm anti}/dP$ is positive for the $A^{1+}B^{5+}O_3^{2-}$

compounds and for most of the $A^{2+}B^{4+}O_3^{2-}$ family members. Note also that $CaSiO_3$,$SrGeO_3$, and $SrMnO_3$ have negative dR_{anti}/dP and relatively large tolerance factors, which is at odds with the rule proposed by Angel *et al.* [22].

Figure 1 thus indicates that the pressure behavior of the tilting angle can be typically understood if (i) one considers the decrease of dR_{anti}/dP with the tolerance factor within a family series, including the possibility that dR_{anti}/dP changes sign as the tolerance factor increases; and (ii) for similar values of the tolerance factor, $A^{1+}B^{5+}O_3^{2-}$ and $A^{2+}B^{4+}O_3^{2-}$ compounds have larger dR_{anti}/dP than $A^{3+}B^{3+}O_3^{2-}$ materials. However, these two rules are not the full story, as for example they cannot explain why $CaTiO_3$ has a larger dR_{anti}/dP than $CaSnO_3$ while the tolerance factor of the latter is smaller than that of the former, both belonging to the $A^{2+}B^{4+}O_3^{2-}$ family and having the same A cation. As we will show below, this exotic behavior is related to the presence of fully empty low-lying d states in some $A^{2+}B^{4+}O_3^{2-}$ materials. In addition, $SrTiO_3$ presents a larger dR_{anti}/dP value than $CaTiO_3$, which is also against the usual trend that dR_{anti}/dP decreases with the tolerance factor for a given series. This is because the magnitude of dR_{anti}/dP is enhanced in systems with small tiltings, as we will discuss later in detail.

Although dR_{in}/dP presents essentially the same trends as dR_{anti}/dP, there is a notable difference: the magnitude of dR_{in}/dP (i.e., $|dR_{in}/dP|$) is larger than that of dR_{anti}/dP for systems having large tolerance factor. For example, $|dR_{in}/dP|$ is much larger than $|dR_{anti}/dP|$ in $SrTiO_3$ and $LaAlO_3$. We show below that this is because in-phase tilts are much smaller than antiphase tilts in compounds with large tolerance factor.

It is also important to recall that some perovskite materials might display antiphase tiltings about two or three different pseudocubic ⟨001⟩ directions. For instance, $LaAlO_3$ adopts a rhombohedral structure ($R\bar{3}c$ space group) with tiltings about all three pseudocubic ⟨001⟩ axes. Our calculations (Fig. S1 of the Supplemental Material [29]) indicate that the effect of pressure on the antiphase tiltings in $R\bar{3}c$ perovskites is qualitatively similar to the one for rotations about a single ⟨001⟩ axis, depicted in Fig. 1(b).

B. Cases combining antiphase and in-phase rotations

Interestingly, in-phase and antiphase tiltings are simultaneously present in many perovskites. In fact, such is the case of the most common perovskite structure, the so-called $GdFeO_3$ type. This phase is orthorhombic with the *Pbnm* space group and results from the condensation of an antiphase tilt about the [110] pseudocubic axis (R_5^- mode) and an in-phase rotation about the [001] pseudocubic axis (M_2^+ mode) with respect to the ideal cubic perovskite structure. According to Glazer's notation [9], the tilting in the *Pbnm* structure can therefore be described as $a^-a^-c^+$. In this *Pbnm* structure, A-site antipolar displacements (X_5^- mode) are allowed by symmetry, which optimize the A-site cation coordination environment and further stabilize this phase [30–34].

Our extensive DFT calculations on *Pbnm* compounds reveal that orthorhombic perovskites can adopt rather different pressure behaviors of octahedral tiltings. To demonstrate that, Fig. 2 shows the pressure dependence of the magnitude of the two octahedral tiltings (R_5^- and M_2^+ mode) in four selected

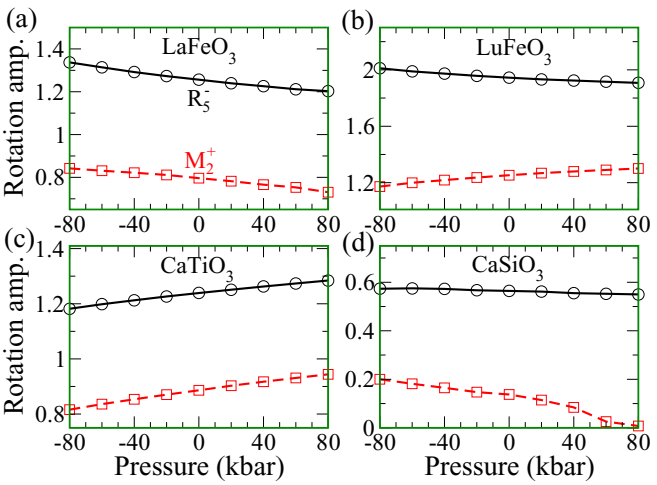

FIG. 2. Pressure effect on octahedral tiltings in *Pbnm* (a) $LaFeO_3$, (b) $LuFeO_3$, (c) $CaTiO_3$, and (d) $CaSiO_3$. The behaviors of both R_5^- mode (antiphase tilt about the [110] axis) and M_2^+ mode (in-phase tilt about the [001] axis) are shown.

materials, namely $LaFeO_3$,$LuFeO_3$,$CaTiO_3$, and $CaSiO_3$. The symmetry-mode decomposition is carried out with the ISODISTORT program [35]. Pressure suppresses both in-phase and antiphase tiltings in $LaFeO_3$. In contrast, we find that, in the case of $CaTiO_3$, pressure enhances both in-phase and antiphase rotations, in agreement with the experimental result of Ref. [15]. Strikingly, the pressure behavior of the tilts in $LuFeO_3$ is still different: pressure suppresses the antiphase mode but enhances the in-phase rotation. Note also that other test calculations (not shown here) indicate that *Pbnm* $A^{3+}B^{3+}O_3^{2-}$ compounds with a small A-site ion (i.e., $LuAlO_3$,$TmFeO_3$,$LuCrO_3$) displays a similar behavior to $LuFeO_3$. Therefore, besides the two well-known behaviors that pressure enhances or suppresses both in-phase and antiphase tiltings, we discover that it can also suppress the antiphase R_5^- mode and enhance the in-phase M_2^+ mode in *Pbnm* compounds with a small tolerance factor.

Figure 2 further indicates that, for $CaSiO_3$, hydrostatic pressure suppresses both R_5^- and M_2^+ modes. This is in agreement with the computational work of $CaSiO_3$ [23], but contradicts the general rule proposed by Angel *et al.* [22] which states that the octahedral tiltings in all $A^{2+}B^{4+}O_3^{2-}$ perovskites are enhanced under pressure.

C. Landau-like description

Let us now introduce an elementary Landau-like potential to describe the energetics of the in-phase and antiphase tilting instabilities, which will be useful for the discussion that follows.

Since octahedral rotations can either be in-phase or antiphase and can also be along three different pseudocubic ⟨001⟩ directions, there are six elementary octahedral tilting modes that are $R_{in}^x, R_{in}^y, R_{in}^z$ (which represent the in-phase tilt, M_2^+, about the pseudocubic [100], [010], and [001] axis, respectively) and $R_{anti}^x, R_{anti}^y, R_{anti}^z$ (which are associated with the antiphase tilt, R_5^-). Using group theory, we can derive the energy series (up to the fourth order in the tilting amplitudes)

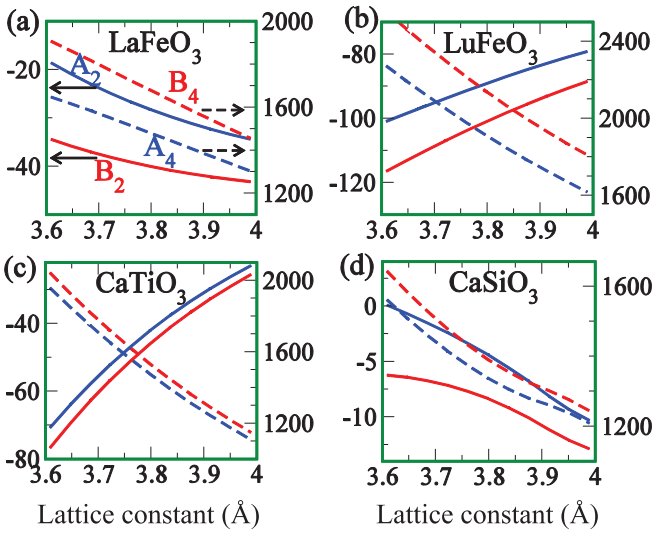

FIG. 3. Dependence of the coefficients (A_2, B_2, A_4, B_4) of the energy model [Eq. (1)] on the lattice constant. The coefficients A_2, A_4, B_2, B_4 are in unit of eV/formula-unit. Four cases [(a) $LaFeO_3$, (b) $LuFeO_3$, (c) $CaTiO_3$, and (d) $CaSiO_3$] are shown.

for the distorted perovskite structure:

$$E_{\text{tilt}} = A_2 \sum_{\alpha} \left(R^{\alpha}_{\text{in}}\right)^2 + A_4 \sum_{\alpha} \left(R^{\alpha}_{\text{in}}\right)^4 + B_2 \sum_{\alpha} \left(R^{\alpha}_{\text{anti}}\right)^2 + B_4 \sum_{\alpha} \left(R^{\alpha}_{\text{anti}}\right)^4 + E^4_{\text{cross}}, \quad (1)$$

where $\alpha = \{x, y, z\}$, the coefficients A_2 and A_4 (respectively, B_2 and B_4) describe the energy landscape for in-phase (respectively, antiphase) tilts, and E^4_{cross} gathers all the fourth-order (including biquadratic) coupling terms between these six tilting modes. The six elementary octahedral tilting modes are adopted as independent variables in order to make this Landau-like potential as general as possible. Our DFT calculations show that all these fourth-order coupling terms E^4_{cross} are positive and increase with pressure for all perovskites considered in this paper, suggesting that the antiphase and in-phase tilt modes compete with each other and that this competition is enhanced by pressure. Since the pressure behavior of E^4_{cross} is similar to that of the fourth-order A_4 and B_4 terms, we will not discuss them hereafter.

The A_2, A_4, B_2, and B_4 coefficients are fitted to DFT results (see Appendix for the computational details). We plot them in Fig. 3 as a function of the pseudocubic five-atom-cell lattice constant for the four materials studied in Fig. 2. It can be seen that the fourth-order coefficients (A_4 and B_4) are always positive and increase with pressure (i.e., when decreasing the lattice constant), which is expected since the octahedral tilting will reduce the distance between the next-nearest-neighboring (NNN) oxygen ions, as well as the A-O distance, resulting in a stronger short-range (Pauli) repulsion associated to overlapping electrons of different atoms. The second-order coefficients (A_2 and B_2) are negative, as consistent with instability of the tilts, and display a much richer behavior. They decrease for $LaFeO_3$ and $CaSiO_3$, resulting in weaker tilting instabilities for increasing pressure. The reverse trend occurs in $CaTiO_3$ and $LuFeO_3$. Note that the tilt magnitude in a $a^0a^0c^-$ (respectively, $a^0a^0c^+$) structure is given by $R^{\text{min}}_{\text{anti}} = \sqrt{\frac{-B_2}{2B_4}}$ (respectively, $R^{\text{min}}_{\text{in}} = \sqrt{\frac{-A_2}{2A_4}}$). Since $|A_2|$ and $|B_2|$ decrease with pressure in $LaFeO_3$ and $CaSiO_3$ and the fourth-order coefficients always increase with pressure, it follows that the O_6 rotations must decrease under compression, as shown in Fig. 2. In contrast, for $CaTiO_3$ and $LuFeO_3$, there is a competition between the second- and fourth-order terms. In $CaTiO_3$, the tilts increase with pressure because the change of the second-order coefficient is faster than that of the fourth-order coefficient. The case of $LuFeO_3$ is more subtle because the behavior of the second- and fourth-order terms indicated in Fig. 3 should result in a decrease of both in-phase and antiphase tilts; this is consistent with the result for single-tilt cases shown in Fig. 1, but contradicts our results for the *Pbnm* structure in Fig. 2. This apparent contradiction hints at an interaction between in-phase and antiphase tilts in $LuFeO_3$, which, as we will see later, corresponds to the existence of a trilinear coupling involving both octahedral tilts together with an antipolar distortion mode.

III. DISCUSSION

Let us now try to better understand the results displayed in Figs. 1 and 2 and unravel the origins of the different pressure behaviors of the oxygen octahedral tiltings. For that, it is important to consider the following aspects.

A. Origin of the octahedral tilting instabilities

1. *Dominant interatomic interactions that drive the octahedral tilt instabilities*

It is widely accepted that the instability of octahedral tilting in ABO_3 perovskites is due to the tendency to increase the A-O interactions, either covalent or electrostatic [10]. Let us test such a notion against our first-principles calculations.

To do this, we first propose an original way to decompose the second-order Landau coefficients [A_2 and B_2 in Eq. (1)] into different contributions. Note that these coefficients are directly related to the (harmonic) force constants describing the energy changes for small distortions of the ideal cubic perovskite phase of the material. More specifically, we have

$$E_2 = \frac{1}{2} \sum_{lk\alpha} \sum_{l'k'\beta} \Phi_{\alpha\beta}(lk, l'k') u_{\alpha}(lk) u_{\beta}(l'k'), \quad (2)$$

where $u_{\alpha}(lk)$ is the atomic displacement along the α direction of the kth atom in the lth unit cell, and Φ are the harmonic force constants. For the particular case of a O_6-tilting distortion, only the oxygen atoms move, and we can write $E_2 = E_2^{\text{self}} + E_2^{\prime\text{O-O}}$, where the first term comes from the self-interaction of the oxygen atoms ($lk = l'k'$) and the second one includes all the couplings between couples of different oxygens ($lk \neq l'k'$) in Eq. (2). Now the self-energy of a particular atom can be actually interpreted as an interaction with the rest of the lattice, by means of the acoustic sum rule $\Phi_{\alpha\beta}(lk, lk) = -\sum_{l'k' \neq lk} \Phi_{\alpha\beta}(lk, l'k')$, where $l'k' \neq lk$ in the sum. Hence, we can use this expression to expand E_2^{self} and, by grouping together the terms involving O-O, O-A, and O-B atomic pairs, we can split the energy as $E_2 = E_2^{A\text{-O}} + E_2^{B\text{-O}} + E_2^{\text{O-O}}$, where it should be noted that $E_2^{\text{O-O}}$ contains the interactions in the

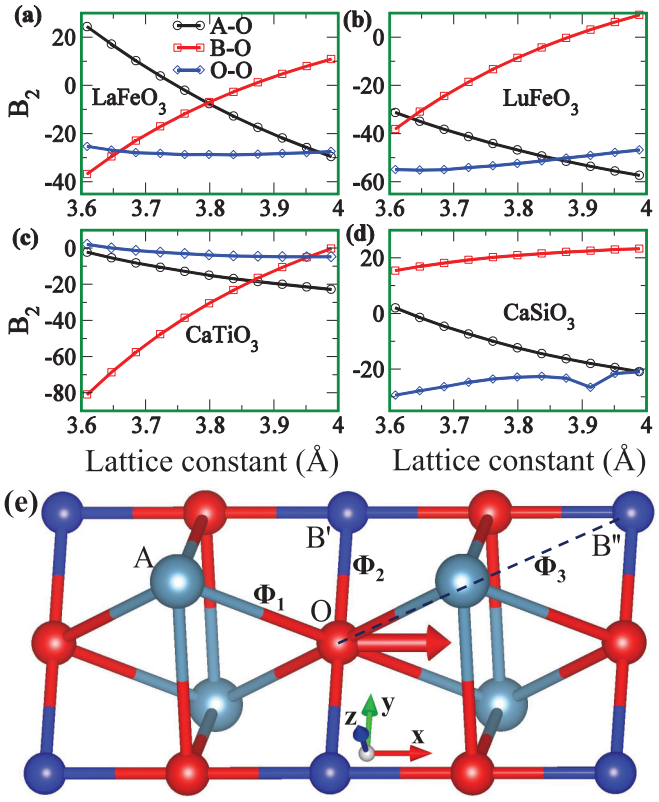

FIG. 4. Contributions ($B_2^{A\text{-}O}$, $B_2^{B\text{-}O}$, and $B_2^{O\text{-}O}$) from different interactions to B_2 of the energy model [Eq. (1)] as a function of lattice constant. The coefficients B_2 are in unit of eV/formula-unit. Four cases [(a) $LaFeO_3$, (b) $LuFeO_3$, (c) $CaTiO_3$, and (d) $CaSiO_3$] are shown. The local environment for an oxygen moving along the x direction (due to a octahedral rotation about z) is shown in panel (e). Φ_1, Φ_2, and Φ_3 represent the A-O, B'-O, and B''-O force constants, respectively.

$E_2'^{O\text{-}O}$ energy introduced above, plus additional contributions coming from the self-energy.

In terms of the decomposed energies, one can write the individual contribution to B_2 as $B_2^{P\text{-}P'} = E_2^{P\text{-}P'}/R^2$, where R is the amplitude of the tilting and P-P' represents a particular pair of atom types. Note that negative values of $B_2^{P\text{-}P'}$ indicate that the P-P' interaction favors octahedral tilting. The separated contributions to B_2 for the four compounds in Fig. 2 are shown in Fig. 4. We can see that there is a significant B-O contribution to B_2 besides the expected A-O and O-O contributions. Moreover, $B_2^{A\text{-}O}$ increases under compression while $B_2^{B\text{-}O}$ decreases and $B_2^{O\text{-}O}$ is weakly pressure dependent. Interestingly, both $B_2^{A\text{-}O}$ and $B_2^{B\text{-}O}$ can change sign as a function of pressure. In particular, for $LaFeO_3$, $B_2^{A\text{-}O}$ becomes positive for lattice constants smaller than 3.75 Å, indicating that the A-O interaction is then unfavorable for the occurrence of octahedral tilts. At the same time, in $LaFeO_3$ $B_2^{B\text{-}O}$ becomes negative and larger in magnitude than $B_2^{A\text{-}O}$, implying that the octahedral tilt instability is now driven by the B-O and O-O interactions [see Fig. 4(a)]. As a result, the B-O contribution becomes more and more important for the condensation of oxygen octahedral tiltings under pressure in $LaFeO_3$. Note that a similar conclusion can be drawn for $CaTiO_3$ and to a lesser extend to $LuFeO_3$, according to Fig. 4.

In order to understand how the B atoms drive the octahedral tilt, we analyze the force constants in more detail. Around each oxygen, there are two nearest-neighboring (NN) B ions and eight NNN B ions [B' and B'' in Fig. 4(e), respectively]. Without loss of generality, we assume that the central oxygen atom is moving along the x direction when the tilt occurs. Taking $LaFeO_3$ with the lattice constant of 3.8 Å as a typical example, we find that force constant between B' and O along the x direction is $\Phi_2 = -0.78$ eV/Å^2, while the coupling between B'' and O along the x direction is $\Phi_3 = 1.01$ eV/Å^2. For comparison, the force constant between O and its NN A ion along the x direction is $\Phi_1 = 0.16$ eV/Å^2. A negative value of Φ_2 results in a positive contribution to $E_2^{B\text{-}O}$ and is consistent with the observation that the octahedral tilt makes the NN B-O interaction less favorable. Surprisingly, the force constant between O and its NNN B ion is even larger than that between O and its NN A ion, and of opposite sign; hence, upon condensation of the tilting distortion, the energy reduction associated to the NNN B-O interaction will be larger than the energy penalty coming from the NN A-O interaction. Note that the tilting will bring the O atoms and its NNN B atoms closer, thus optimizing the covalent and/or electrostatic factors contributing to the interaction. When the A site has a large ionic radius or the B ion could form a strong covalent bond with oxygen, the NNN B-O interaction is more important than the NN A-O interaction even though the NNN B-O distance is larger than the NN A-O distance. Therefore, we find that the interaction between the NNN B-ion and oxygen ion is another important source of the octahedral tilting instability. Note that this may explain why the octahedral tilting also occurs in materials that, like α-AlF_3 [36], do not contain any A-site cations. Interestingly, the effect of the interaction between the NNN B ion and oxygen ion on octahedral tilting becomes more and more significant under pressure. This also explains our numerical finding that pressure enhances octahedral tiltings in α-AlF_3.

2. *Why does the antiphase tilting usually have a stronger instability than the in-phase tilting?*

Experiments show that antiphase tilts occur more frequently than in-phase tilts in perovskites. For example, $SrTiO_3$ takes the $I4/mcm$ tetragonal structure with a single antiphase tilt at low temperature. In contrast, to our best knowledge, a perovskite compound never adopts the structure with a single in-phase tilt as the ground state. This is because the instability of the antiphase tilt is stronger than that of the in-phase tilt (that is, $B_2 < A_2$) for a given lattice constant, as shown in Fig. 3. By computing the electrostatic energy with the Ewald method, we find that this is caused by a larger gain in O-O electrostatic energy in the antiphase case. By decomposing the second-order coefficients A_2 and B_2 into different contributions with the use of second-order force constants, we find that $A_2^{A\text{-}O} = B_2^{A\text{-}O}$ and $A_2^{B\text{-}O} = B_2^{B\text{-}O}$, while $A_2^{O\text{-}O} > B_2^{O\text{-}O}$. Therefore, the O-O interaction favors antiphase tilt over in-phase tilt.

B. Pressure-dependence of simple oxygen octahedral rotational patterns

1. *Influence of ionic sizes*

Let us now explain why dR/dP for the compounds in a given series usually decreases with the tolerance factor, as

shown in Fig. 1. A small tolerance factor indicates that B and oxygen atoms will be tightly packed, while the A atoms will be relatively loose. This suggests that the BO_6 octahedron will be less compressible than the AO_{12} polyhedron for perovskites with small tolerance factor. When pressure is applied, the material will thus tend to shorten the A-O bonds while maintaining the distance between B and O atoms, i.e., the octahedral tiltings will tend to increase. If the tolerance factor is large, the opposite applies and pressure suppresses the octahedral tilting. This argument is in agreement with the fact that B_2 for $LaFeO_3$ decreases with the lattice constant, while B_2 for $LuFeO_3$ increases [see Figs. 3(a) and 3(b)]. Figure 4 shows that this is because $B_2^{A\text{-O}}$ increases much faster with decreasing lattice constant in $LaFeO_3$ than in $LuFeO_3$, which probably reflects the fact that the electrons of the relatively large La^{3+} cations quickly start to repel the O^{2-} anion under pressure. Thus, this electronic repulsion is the most likely explanation for the observation that dR/dP usually decreases with the tolerance.

2. *Influence of ionization states*

As we discussed above, pressure usually suppresses the octahedral tilting in $A^{3+}B^{3+}O_3^{2-}$ compounds, while enhancing it in $A^{2+}B^{4+}O_3^{2-}$ materials (see Fig. 1). Such an effect was previously explained in terms of the bond-valence parameters [22]. Here, we would like to rather suggest that this effect is due to the dependence of the A-O interaction on the formal charge of the A ion. Generally speaking, the ionic radius of A cations with a high valence is smaller than that of cations with a low valence [27] since more strongly charged cations will tend to move closer to the anion in order to lower the electrostatic energy. For example, the ionic radii of Rb^{1+}, Sr^{2+}, and Y^{3+} are 1.66, 1.32, and 1.04 Å, respectively. The distance between oxygen and A ions with a high valence is thus already small at zero pressure, implying that the corresponding A-O bond will be relatively hard to compress. Such a notion is demonstrated in Fig. S3 [29], where $B_2^{A\text{-O}}$ is found to increase much faster with decreasing volume in $LaAlO_3$ than in $CaGeO_3$, despite the fact that they have similar tolerance factors. This explains why, for materials with similar tolerance factors, $\frac{dR}{dP}$ usually decreases as we move from $A^{1+}B^{5+}O_3^{2-}$ to $A^{2+}B^{4+}O_3^{2-}$ and then to $A^{3+}B^{3+}O_3^{2-}$.

3. *Influence of orbital hybridizations*

Figures 1 and 2 show that $\frac{dR}{dP}$ for $CaTiO_3$, $CaZrO_3$, $CaHfO_3$, and $SrTiO_3$ is much larger than for $CaBO_3$(B = Si, Ge, Sn, or Mn) and $SrBO_3$(B = Ge or Mn), at variance with the usual trend with respect to the tolerance factor. Interestingly, the key difference between these compounds is that $CaTiO_3$, $CaZrO_3$, $CaHfO_3$, and $SrTiO_3$ have empty low-lying d states, while the others do not. We thus decided to examine whether the empty d states play a role on the effect of pressure on octahedral tiltings.

To isolate the effect of the hybridization between the empty d states and the O-2p states on the octahedral tilting, we employ the orbital selective external potential (OSEP) method [37,38], in which an external field is applied to shift the energy levels of some chosen orbitals. More precisely, we shift the

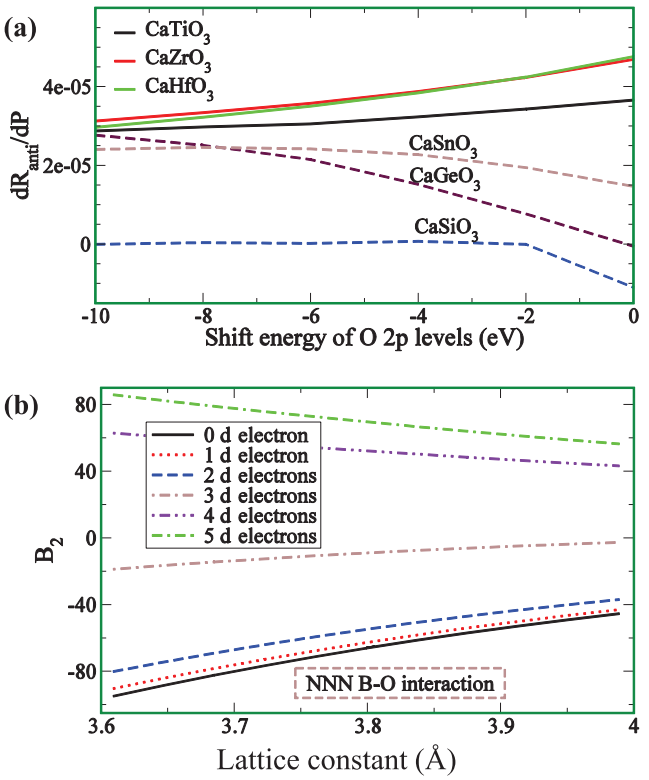

FIG. 5. Origin of the pressure enhancement of octahedral rotations in ABO_3 compounds with low-lying d states of B site. (a) Derivative of antiphase rotation with respect to pressure as a function of the shifted energy of oxygen 2p states. When the shift energy is more than -2eV, $CaSiO_3$ becomes cubic with $R_{\text{anti}} = 0$ and $\frac{dR_{\text{anti}}}{dP} = 0$. (b) Contribution from the NNN B-O hybridization to B_2 of the energy model [Eq. (1)] from the TB calculation. One can see that the NNN B-O interaction makes B_2 much more negative when the lattice constant decreases in systems with low occupation of the d orbitals.

O-2p states to a lower level so that their hybridization with the empty states of the B ion decreases. As can be seen from Fig. 5(a), dR_{anti}/dP for $CaBO_3$ (B = Ti, Zr, and Hf) becomes smaller for lower-lying O-2p levels. The opposite trend is observed for $CaBO_3$ compounds (B = Si, Ge, and Sn). Therefore, it is clear that the hybridization between the empty d states of the B ion and the O-2p states is a key factor leading to larger dR_{anti}/dP values for $CaTiO_3$, $CaZrO_3$, and $CaHfO_3$.

Let us now try to understand why this is the case. For that, we carry out tight-binding (TB) calculations, considering a $R\bar{3}c$ phase of $CaTiO_3$ as a representative model system. In our TB Hamiltonian, we consider the Ti-3d orbitals and O-2p orbitals. The hopping integrals t are evaluated with the Slater-Koster scheme [39]. Following Harrison [40], we adopt $t \propto \frac{1}{d^{5/2}}$ to take into account the dependence on the interatomic distance. We compute the energy given by this model (this is simply the band energy $E_b = \sum_k \sum_{i=1}^{n_{\text{occ}}} \varepsilon_{ik}$, where n_{occ} is the number of occupied bands and ε_{ik} is the eigenvalue of the ith band at k-point $\boldsymbol{k}$ for two cases). In the first case, we only consider the NN Ti-O hopping t_{NN}, while in the second case we also include the NNN Ti-O hopping $t_{\text{NNN}} = t_{\text{NN}}(\frac{d_{\text{NN}}}{d_{\text{NNN}}})^{5/2}$, where d_{NN} and d_{NNN} are the

NN Ti-O distance and NNN Ti-O distances, respectively. We thus find that the NNN B-O interaction makes B_2 much more negative when the lattice constant is small, i.e., under pressure [see Fig. 5(b)], which can be explained as follows. When a pressure is applied, the NNN Ti-O interatomic distance is reduced, and the hopping between the O-2p orbitals and Ti-3d orbitals is thus enhanced significantly. Therefore, the hybridization between the Ti-3d and the O-2p orbitals makes the second-order coefficients (A_2 and B_2) more negative, increasing the tendency of octahedral tilting under pressure. Note that, when there are too many filled d electrons, the NNN B-O interaction might increase B_2 for decreasing lattice constant [see Fig. 5(b) for the four and five d electrons/B-site cases]. This explains why the p-d hybridization plays a less important role on the octahedral tilts in $RE\mathrm{CrO_3}$,$\mathrm{CaMnO_3}$, and $\mathrm{SrMnO_3}$ systems. Hence, this analysis suggests that having empty low-lying d states plays a significant role in the pressure behavior of octahedral tilting in perovskites. Recently, it was pointed out that the tolerance factor alone does not determine the temperature at which the cubic phase is stabilized and that the electronic configuration of the B-site cation appears to also be of significance [41]. This is in agreement with our present finding that the d-orbital occupation is also relevant to the octahedral tilting. By considering the NN B-O interaction, Woodward proposed that the B-Oπ-bonding favors the cubic perovskite ABO_3 structure if the $\pi^* t_{2g}$ d band is filled and less than half-filled [10]. In contrast, here, we consider the role of the NNN B-O interaction.

4. *Influence of magnitude of the octahedral tilting*

Figure 1 shows that $\mathrm{SrTiO_3}$ has a larger dR/dP than $\mathrm{CaTiO_3}$, and that $|dR_{\mathrm{in}}/dP|$ is much larger than $|dR_{\mathrm{anti}}/dP|$ in $\mathrm{SrTiO_3}$, $\mathrm{LaAlO_3}$, $\mathrm{CaSiO_3}$, and $\mathrm{SrMnO_3}$. To be more specific, dR_{in}/dP is more negative than dR_{anti}/dP in $\mathrm{LaAlO_3}$, $\mathrm{CaSiO_3}$, and $\mathrm{SrMnO_3}$, while $dR_{\mathrm{in}}/dP > dR_{\mathrm{anti}}/dP > 0$ in $\mathrm{SrTiO_3}$. These unusual behaviors cannot be explained by the three effects we just discussed above. An indication appears to be that this phenomenon happens when the tilt at zero pressure is small. For simplicity, let us consider the in-phase tilting case. Since the magnitude of tilt at zero pressure can be computed as $R_{\mathrm{in}} = \sqrt{\frac{-A_2}{2A_4}}$, we have $dR_{\mathrm{in}}/dP = \frac{1}{2R_{\mathrm{in}}} d(\frac{-A_2}{2A_4})/dP$. This suggests that the magnitude of dR_{in}/dP is inversely proportional to the magnitude of the tilts. In fact, the in-phase tilts in all these four compounds ($\mathrm{SrTiO_3}$, $\mathrm{LaAlO_3}$, $\mathrm{CaSiO_3}$, and $\mathrm{SrMnO_3}$) are numerically found to be very small. Our DFT calculations also predict that $\mathrm{CaTiO_3}$ has an even slightly larger $|d(\frac{-A_2}{2A_4})/dP|$ than $\mathrm{SrTiO_3}$ (not shown here), which further suggests that the reason why $\mathrm{SrTiO_3}$ has a larger $|dR_{\mathrm{in}}/dP|$ than $\mathrm{CaTiO_3}$ is that $\mathrm{SrTiO_3}$ has a much smaller in-phase tilt than $\mathrm{CaTiO_3}$.

C. Cases combining in-phase and antiphase rotations

So far, we have discussed the behavior of simple structures in which only one type of tilting pattern, in-phase or antiphase, exists. The observed trends should be applicable to cases combining in-phase and antiphase rotations, as those shown in Fig. 2. However, there is another effect displayed in Fig. 2 that cannot be explained by the above considerations, that is, why pressure suppresses the antiphase R_5^- mode but simultaneously enhances the in-phase M_2^+ mode in *Pbnm* $\mathrm{LuFeO_3}$. First, it is important to realize that, according to our numerical results, the strain degree of freedom is not the key to this behavior, as evidenced in Fig. S4 of the Supplemental Material [29]. Therefore, we hereafter focus on the cubic cell for simplicity and recall that the *Pbnm* state also displays antipolar motions of the A cations. Interestingly, we numerically find that, if we suppress such antipolar motions, by fixing the A ion to their ideal high-symmetry positions, pressure suppresses both the antiphase mode and in-phase rotations in *Pbnm* $\mathrm{LuFeO_3}$, in agreement with the behavior of the tilting patterns considered individually that we found for this compound [see Figs. 1(a) and 1(b)]. Therefore, a coupling between the A site related antipolar mode (of X_5^- symmetry) with the rotational modes (R_5^- and M_2^+) should be responsible for the exotic behavior of $\mathrm{LuFeO_3}$ under pressure. Interestingly, it has been recently shown that there is a specific trilinear coupling between the three modes existing in any *Pbnm* perovskite [30]. Incorporating such coupling in a simple model gives

$$\begin{aligned} E &= E_{\mathrm{tilt}} + E(X) + E_c, \\ \text{with} \quad E_{\mathrm{tilt}} &= E(R) + E(M) + E(R,M) \quad \text{and} \\ E_c &= E(X,R) + E(X,M) + \lambda XRM, \end{aligned}$$

where R and M represent the amplitude of the tilting patterns $a^-a^-c^0(R_5^-)$ and $a^0a^0c^+(M_2^+)$, respectively; X denotes the amplitude of the X_5^- mode; and we also have individual mode energies $E(M) = A_2^M M^2 + A_4^M M^4$, $E(R) = B_2^R R^2 + B_4^R R^4$, and $E(X) = C_2^X X^2 + C_4^X X^4$; finally, λ denotes the strength of the trilinear coupling and note that, for simplicity, we do not consider strains in the model. The fourth-order repulsion terms $E(P,Q)$ take the form of $P^2Q^2(P,Q = X,R \text{ or } M$ and $P \neq Q)$. Note that B_2^R and B_4^R are related to, but different from, B_2 and B_4 in Eq. (1), since the $a^-a^-c^0$-like distortion is an antiphase octahedral rotation about both the pseudocubic x and y axes.

By fitting this model energy to DFT results, we obtain the corresponding parameters at different pressures. Note that, for these DFT simulations, we consider structures in which the cell is forced to be cubic, but the atoms move from their high-symmetry positions as in a regular *Pbnm* phase. At each pressure, the lattice constant of the cubic cell is chosen so that the cell volume is the one obtained for the actual *Pbnm* structure of $\mathrm{LuFeO_3}$ with an orthorhombic cell. Some of these fitted parameters are shown in Fig. 6(a). The fourth-order coefficients A_4^M and B_4^R are positive and increase with pressure. It is important to note that B_4^R grows faster than A_4^M, suggesting that the antiphase tilt becomes less favorable than the in-phase rotations under pressure. We also find (not shown here) that (i) as expected, A_2^M and B_2^R decrease with pressure, in agreement with our above results for the second-order coefficients A_2 and B_2 in Fig. 3; and (ii) C_2^X is negative, indicating that the X_5^- mode itself is an instability of the cubic phase of $\mathrm{LuFeO_3}$. This is different from the usual case (e.g., $\mathrm{LaGaO_3}$) where the X_5^- mode itself is stable and its occurrence in the *Pbnm* structure is induced by the trilinear coupling [30,34]. The small size of Lu^{3+} (and the small tolerance factor of $\mathrm{LuFeO_3}$) are surely responsible for this behavior. Interestingly, we also find that the magnitude of the trilinear coupling $|\lambda|$

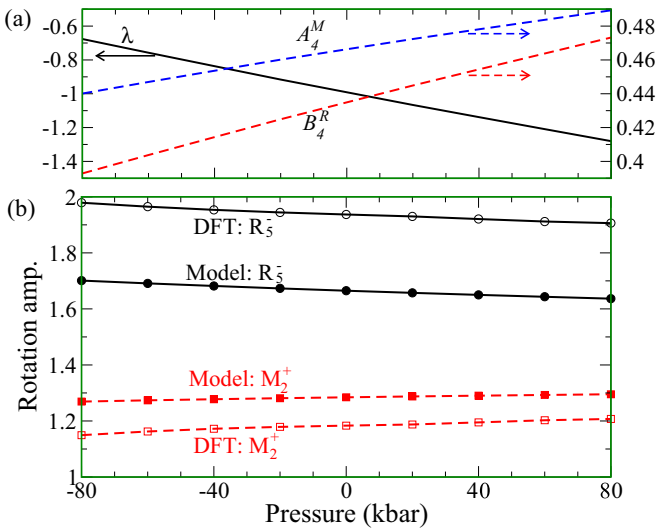

FIG. 6. Explanation for the pressure behavior of octahedral tilt in *Pbnm* $LuFeO_3$. (a) Parameters (λ denotes the trilinear coupling strength, A_4^M and B_4^R are fourth-order coefficients of in-phase rotation and antiphase rotation, respectively) of the energy simple model incorporating the trilinear coupling, as a function of pressure. (b) Amplitude of the in-phase and antiphase rotations as a function of pressure from the DFT calculation and the energy model. Since the strain degree of freedom is not crucial for the pressure behavior of octahedral tilt (see Fig. S4 of the Supplemental Material [29]), the cell is kept cubic here.

increases rapidly with pressure [see Fig. 6(a)]. Furthermore, in Fig. 6(b), we report the amplitude of the R_5^- and M_2^+ modes as obtained from the DFT calculations and reproduced by our simple model. While the qualitative agreement is good, there are quantitative discrepancies that are probably due to the fourth-order truncation of our model potential.

Let us now discuss the origin of the differentiated behavior of in-phase and antiphase tiltings under pressure in $LuFeO_3$. We numerically found that, when removing the pressure dependence of the trilinear coupling (i.e. making λ constant equal to its value at zero pressure), both the in-plane and antiphase tilts are suppressed by pressure. Further, the reason why the pressure enhances the in-phase M_2^+ mode, but suppresses the antiphase R_5^- mode, is that the B_4^R coupling increases faster with pressure than A_4^M. Indeed, if we make the pressure dependence of B_4^R identical to that of A_4^M, our model predicts that pressure would then enhance the R_5^- mode and suppress the M_2^+ distortion. Furthermore, increasing the pressure dependence of A_4^M to make it equal to that of B_4^R leads to a suppression of both the R_5^- and M_2^+ distortions.

Hence, we find that the peculiar behavior of $LuFeO_3$ relies on a complex interplay among the anharmonic couplings A_4^M, B_4^R, and λ and their pressure dependence. In particular, the enhancement of the trilinear coupling under pressure and faster hardening of the antiphase distortions are responsible for the observed behavior of this compound.

D. Rules for the pressure effect on octahedral tilting

From our above discussion, we are now in a position to propose the following rules governing the effect of pressure on octahedral tilting in perovskites. (I) The derivative of the tilting angles with respect to pressure ($\frac{dR}{dP}$) decreases when increasing tolerance factor. (II) For materials with similar tolerance factors, $\frac{dR}{dP}$ increases as we move from $A^{3+}B^{3+}O_3^{2-}$ to $A^{2+}B^{4+}O_3^{2-}$ and finally to $A^{1+}B^{5+}O_3^{2-}$ compounds. (III) Perovskites in which the B-site transition metal presents low-lying empty d states display relatively large values of $\frac{dR}{dP}$, as compared to similar compounds (similar tolerance factors, same nominal ionization states) in which this condition is not fulfilled. (IV) Materials with small tilting instabilities tend to display larger $|\frac{dR}{dP}|$ values than similar compounds (similar tolerance factors, same nominal ionization states) in which the O_6 rotations are large.

Note that rules I and II are implied in the literature, while rules III and IV are proposed here. Furthermore, the physical origins of all four rules are revisited or shown in this paper. For instance, rule I follows from the fact that the A-site-driven octahedral tilting instabilities decrease quickly under pressure if the A cation is large. Rule II originates from the fact that A cations in a high ionization state have smaller radii and are harder to compress than A ions in a low ionization state. We find that rule III applies because NNN B-O covalent interactions are enhanced when octahedral tilt increases under pressure. Finally, rule IV follows from the fact that the magnitude of dR/dP is roughly inversely proportional to the magnitude of the tilt.

In addition, we observe that pressure can also enhance the in-phase octahedral tilting, but suppress the antiphase octahedral tilting, in orthorhombic perovskites having a small tolerance factor. Such an effect strongly relies on the trilinear energy coupling among the in-phase tilt, the antiphase tilt, and an antipolar displacement of the A cations.

E. Relationship with phonon spectrum

Experimentally, the dependency of the frequency of some phonon modes on pressure has often been employed to deduce the effect of pressure on the octahedral tilts. As shown in Figs. S4 and S5 of the Supplemental Material [29], the softening of the low-frequency tilt-related phonon mode always indicates that pressure suppresses the tilt. However, the hardening of the tilt-related phonon modes is not necessarily accompanied by an enhancement of the tilt, as evidenced in the Supplemental Material [29].

F. Further applicability of the formulated rules

In this paper, we focus on perovskite oxides. However, the proposed basic rules should be applicable to other perovskite systems, such as the compounds of the ABF_3 family. For example, we performed DFT calculations on $NaMgF_3$ and found that the octahedral tilting increases with pressure, in agreement with the experimental result of Ref. [42]. Since the tolerance factor is small (0.943) and the B-site ion (Mg^{2+}) has a higher valence than the A-site ion (Na^{1+}), this result is in agreement with rules I and II.

Note that we did not consider the effect of ferroelectric distortions on octahedral tiltings. Since most perovskites are not ferroelectric and the coexistence of ferroelectricity and octahedral tilts is quite rare, our rules should be applicable

to a large number of these materials. We should, however, note that ferroelectricity and octahedral tilts coexist in some systems (e.g., $R3c$ $BiFeO_3$), where the pressure effect on the tilts is left for future investigations. In addition, our rules may not be applicable to orbital-ordered systems, where the coupling between Jahn-Teller distortion and octahedral tilts is also expected to play a role.

As a demonstration of the further applicability of our formulated rules, we will now examine how the so-called hybrid improper ferroelectricity can be affected by pressure. For that, it is important to recall that a trilinear coupling between the two types of octahedral rotation and a polar mode was recently suggested to give rise to this hybrid improper ferroelectricity [31,33,34,43] in ordered perovskites [31,34] and Ruddlesden-Popper compounds [33]. Since the polar mode is induced by two rotational modes, it is expected from this paper that the pressure can tune the hybrid improper ferroelectricity indirectly by controlling the amplitude of the octahedral rotations. As shown in the Fig. S7 of the Supplemental Material [29], we demonstrate this point in 1:1 superlattices made of $CaSiO_3$-$MgSiO_3$ and $LaGaO_3$-$YGaO_3$. In fact, our DFT calculations show that pressure enhances the polarization in the hybrid improper ferroelectricity in $CaSiO_3$-$MgSiO_3$, but suppresses it in $LaGaO_3$-$YGaO_3$, which can be easily understood by recalling the behavior of the octahedral rotations of the parent compounds (see Fig. S7 of the Supplemental Material [29]).

Note that the Supplemental Material [29] also provides the (subtle) relation between the effect of pressure on octahedral tilting and how strain reacts to this pressure in perovskites, which should be of benefit to experimentalists using x-ray techniques to (indirectly) probe the role of pressure on tiltings.

IV. SUMMARY

To summarize, we have comprehensively investigated how pressure affects octahedral rotations in perovskite oxides. This paper has allowed us to confirm and explain some of the existing empirical rules proposed to govern these behaviors, as well as to reveal and understand additional trends. Thus, this paper provides a detailed guide to understand (and predict) the structural response of the vast majority of perovskite oxides under pressure, which should be especially useful given the importance of these effects and the difficulties involved in their experimental characterization. We have also briefly illustrated the implications of our results and conclusions in what regards other materials' families (e.g., fluorides with the perovskite structure) and materials-design problems (e.g., to tune the so-called hybrid improper ferroelectricity). It is expected that the biaxial strain can also affect the octahedral tiltings, which we will leave for a future study.

ACKNOWLEDGMENTS

Work at Fudan was supported by the National Natural Science Foundation of China (Grant No. 11374056), the Special Funds for Major State Basic Research (Grant No. 2015CB921700), Program for Professor of Special Appointment (Eastern Scholar), Qing Nian Ba Jian Program, and Fok Ying Tung Education Foundation. Work at Arkansas is supported by the U.S. Department of Energy Office of Basic Energy Sciences, under Contract No. ER-46612 (H.X.) and the U.S. AFOSR Grant No. FA9550-16-1-0065 (L.B.). We also acknowledge the Fonds National de la Recherche Luxembourg Grants No. P12/4853155 (M.G., J.I., and J.K.) and No. INTER/MOBILITY/15/9890527 GREENOX (L.B. and J.I.). H.X. thanks Prof. C. G. Duan for sharing the OSEP code and Dr. Ke Xu for a critical reading of the manuscript.

APPENDIX: COMPUTATIONALDETAILS

Our total energy calculations are based on the DFT within the generalized gradient approximation [44] on the basis of the projector augmented wave method [45,46] encoded in the Vienna *ab initio* Simulation Package [47,48]. The plane-wave cutoff energy is set to 500 eV. For $REFeO_3$, the Hubbard on-site repulsion [49] is added for Fe $3d$ orbitals. Following the previous DFT + U studies on similar systems [50–52], the on-site repulsion U and exchange parameter J for Fe are set to 5 and 1 eV, respectively. In the OSEP approach [37,38],we add an extra potential $H_{\text{add}} = |inlm\sigma\rangle\langle inlm\sigma|V_{\text{ext}}$ to the original Kohn-Sham Hamiltonian, where V_{ext} is the applied energy shift, i denotes the atomic site, and n, l, m, and σ are the main quantum number, orbital quantum number, magnetic quantum number, and spin index, respectively.

The model parameters of the Landau potential are estimated by fitting to the DFT results. We first obtain the parameters for each single mode by performing a series of DFT calculations with different amplitudes of the mode. We then obtain the coupling between two modes by using the DFT total energy of the states with two condensed modes and the previously obtained parameters for the single mode. In the trilinear coupling case, we finally extract the coupling parameter λ using the DFT total energy of the state with the coexistence of three modes and the already obtained parameters.

[1] J. G. Bednorz and K. A. Müller, in *Ten Years of Superconductivity: 1980–1990* (Springer, Dordrecht, 1993), pp. 267–271.

[2] E. Dagotto, T. Hotta, and A. Moreo, Colossal magnetoresistant materials: The key role of phase separation, Phys. Rep. **344**, 1 (2001).

[3] M. E. Lines and A. M. Glass, *Principles and Applications of Ferroelectrics and Related Materials* (Clarendon Press, Oxford, 1977).

[4] W. Eerenstein, N. D. Mathur, and J. F. Scott, Multiferroic and magnetoelectric materials, Nature **442**, 759 (2006).

[5] R. Ramesh and N. A. Spaldin, Multiferroics: Progress and prospects in thin films, Nat. Mater. **6**, 21 (2007).

[6] K. F. Wang, J. M. Liu, and Z. F. Ren, Multiferroicity: The coupling between magnetic and polarization orders, Adv. Phys. **58**, 321 (2009).

[7] V. M. Fridkin, *Ferroelectric Semiconductors* (Consultants Bureau, New York, 1980).

[8] R. H. Mitchell, *Perovskites: Modern and Ancient* (Almaz Press, Ontario, 2002).

[9] A. Glazer, The classification of tilted octahedra in perovskites, Acta Crystallogr. Sect. B **28**, 3384 (1972).

[10] P. Woodward, Octahedral tilting in perovskites. II. structure stabilizing forces, Acta Crystallogr. Sect. B **53**, 44 (1997).

[11] J. B. Goodenough, *Localized to Itinerant Electronic Transition in Perovskite Oxides* (Springer, New York, 2001).

[12] T. Aoyama, K. Yamauchi, A. Iyama, S. Picozzi, K. Shimizu, and T. Kimura, Giant spin-driven ferroelectric polarization in $TbMnO_3$ under high pressure, Nat. Commun. **5**, 4927 (2014).

[13] G. A. Samara, T. Sakudo, and K. Yoshimitsu, Important Generalization Concerning the Role of Competing Forces in Displacive Phase Transitions, Phys. Rev. Lett. **35**, 1767 (1975).

[14] J. Zhao, N. L. Ross, and R. J. Angel, Tilting and distortion of $CaSnO_3$ perovskite to 7 GPa determined from single-crystal x-ray diffraction, Phys. Chem. Miner. **31**, 299 (2004).

[15] M. Guennou, P. Bouvier, B. Krikler, J. Kreisel, R. Haumont, and G. Garbarino, High-pressure investigation of $CaTiO_3$ up to 60 GPa using x-ray diffraction and Raman spectroscopy, Phys. Rev. B **82**, 134101 (2010).

[16] M. Guennou, P. Bouvier, J. Kreisel, and D. Machon, Pressure-temperature phase diagram of $SrTiO_3$ up to 53 GPa, Phys. Rev. B **81**, 054115 (2010).

[17] P. Bouvier and J. Kreisel, Pressure-induced phase transition in $LaAlO_3$, J. Phys.: Condens. Matter **14**, 3981 (2002).

[18] N. L. Ross, J. Zhao, and R. J. Angel, High-pressure structural behavior of $GdAlO_3$ and $GdFeO_3$ perovskites, J. Solid State Chem. **177**, 3768 (2004).

[19] N. L. Ross, J. Zhao, and R. J. Angel, High-pressure single-crystal x-ray diffraction study of $YAlO_3$ perovskite, J. Solid State Chem. **177**, 1276 (2004).

[20] N. N. Li, Y. Li, H. Li, R. L. Tang, Y. S. Zhao, D. D. Han, Y. M. Ma, Q. L. Cui, P. W. Zhu, and X. Wang, *In-situ* high pressure x-ray diffraction studies of orthoferrite $SmFeO_3$, Chin. Phys. B **23**, 069101 (2014).

[21] T. Tohei, A. Kuwabara, T. Yamamoto, F. Oba, and I. Tanaka, General Rule for Displacive Phase Transitions in Perovskite Compounds Revisited by First Principles Calculations, Phys. Rev. Lett. **94**, 035502 (2005).

[22] R. J. Angel, J. Zhao, and N. L. Ross, General Rules for Predicting Phase Transitions in Perovskites due to Octahedral Tilting, Phys. Rev. Lett. **95**, 025503 (2005).

[23] B. Magyari-Köpe, L. Vitos, G. Grimvall, B. Johansson, and J. Kollár, Low-temperature crystal structure of $CaSiO_3$ perovskite: An *ab initio* total energy study, Phys. Rev. B **65**, 193107 (2002).

[24] V. S. Bhadram, D. Swain, R. Dhanya, M. Polentarutti, A. Sundaresan and C. Narayana, Effect of pressure on octahedral distortions in $RCrO_3$ (R = Lu,Tb,Gd,Eu,Sm): the role of R-ion size and its implications, Mater. Res. Express **1**, 026111 (2014).

[25] J. Zhao, N. L. Ross, and R. J. Angel, New view of the high-pressure behaviour of $GdFeO_3$-type perovskites, Acta Crystallogr. Sect. B **60**, 263 (2004).

[26] V. M. Goldschmidt, Die gesetze der krystallochemie, Naturwissenschaften **22**, 477 (1926).

[27] R. Shannon, Revised effective ionic radii and systematic studies of interatomic distances in halides and chalcogenides, Acta Crystallogr. Sect. A **32**, 751 (1976).

[28] The rotation amplitude (R_{in} and R_{anti}) is characterized by the corresponding displacement of the oxygen ion divided by the lattice constant of the pseudo-cubic structure.

[29] See Supplemental Material at http://link.aps.org/supplemental/10.1103/PhysRevB.96.054102 for additional insight and data on the effect of pressure on oxygen octahedral tilts.

[30] L. Bellaiche and J. Íñiguez, Universal collaborative couplings between oxygen-octahedral rotations and antiferroelectric distortions in perovskites, Phys. Rev. B **88**, 014104 (2013).

[31] H. J. Zhao, J. Íñiguez, W. Ren, X. M. Chen, and L. Bellaiche, Atomistic theory of hybrid improper ferroelectricity in perovskites, Phys. Rev. B **89**, 174101 (2014).

[32] O. Diéguez, O. E. González-Vázquez, J. C. Wojdeł, and J. Íñiguez, First-principles predictions of low-energy phases of multiferroic$BiFeO_3$, Phys. Rev. B **83**, 094105 (2011).

[33] N. A. Benedek and C. J. Fennie, Hybrid Improper Ferroelectricity: A Mechanism for Controllable Polarization-Magnetization Coupling, Phys. Rev. Lett. **106**, 107204 (2011).

[34] J. M. Rondinelli and C. J. Fennie, Octahedral rotation-induced ferroelectricity in cation ordered perovskites, Adv. Mater. **24**, 1961 (2012).

[35] B. J. Campbell, H. T. Stokes, D. E. Tanner, and D. M. Hatch, ISODISPLACE: A web-based tool for exploring structural distortions, J. Appl. Crystallogr. **39**, 607 (2006).

[36] C. Santanu, C. H. Jonathan, X. Y. Qiu, L. L. Peter, D. S. Sarvjit, J. L. B. Simon, and P. G. Clare, Probing local and long-range structure simultaneously: An *in situ* study of the high-temperature phase transition of α-AlF_3, J. Am. Chem. Soc. **126**, 4756 (2004).

[37] Y. P. Du, H. C. Ding, L. Sheng, S. Y. Savrasov, X. G. Wan, and C. G. Duan, Microscopic origin of stereochemically active lone pair formation from orbital selective external potential calculations, J. Phys.: Condens. Matter **26**, 025503 (2014).

[38] X. G. Wan, J. Zhou, and J. M. Dong, The electronic structures and magnetic properties of perovskite ruthenates from constrained orbital-hybridization calculations, Europhys. Lett. **92**, 57007 (2010).

[39] J. C. Slater, and G. F. Koster, Simplified LCAO method for the periodic potential problem, Phys. Rev. **94**, 1498 (1954).

[40] W. A. Harrison, *Electronic Structure and the Properties of Solids* (Dover, New York, 1989).

[41] B. J. Kennedy, M. Avdeev, H. L. Feng, and K. Yamaura, Phase transitions in strontium perovskites. Studies of $SrOsO_3$ compared to other 4*d* and 5*d* perovksites, J. Solid State Chem. **237**, 27 (2016).

[42] H. Z. Liu, J. Chen, J. Hu, C. D. Martin, D. J. Weidner, D. Häusermann, and H. K. Mao, Octahedral tilting evolution and phase transition in orthorhombic $NaMgF_3$ perovskite under pressure, Geophys. Res. Lett. **32**, L04304 (2005).

[43] E. Bousquet, M. Dawber, N. Stucki, C. Lichtensteiger, P. Hermet, S. Gariglio, J. M. Marc Triscone, and P. Ghosez, Improper ferroelectricity in perovskite oxide artificial superlattices, Nature **452**, 732 (2008).

[44] J. P. Perdew, K. Burke, and M. Ernzerhof, Generalized Gradient Approximation Made Simple, Phys. Rev. Lett. **77**, 3865 (1996).

[45] P. E. Blöchl, Projector augmented-wave method, Phys. Rev. B **50**, 17953 (1994).

[46] G. Kresse and D. Joubert, From ultrasoft pseudopotentials to the projector augmented-wave method, Phys. Rev. B **59**, 1758 (1999).

[47] G. Kresse and J. Furthmüller, Efficient iterative schemes for *ab initio* total-energy calculations using a plane-wave basis set, Phys. Rev. B **54**, 11169 (1996).

[48] G. Kresse and J. Furthmüller, Efficiency of *ab-initio* total energy calculations for metals and semiconductors using a plane-wave basis set, Comput. Mater. Sci. **6**, 15 (1996).

[49] A. I. Liechtenstein, V. I. Anisimov, and J. Zaanen, Density-functional theory and strong interactions: Orbital ordering in Mott-Hubbard insulators, Phys. Rev. B **52**, R5467 (1995).

[50] P. S. Wang and H. J. Xiang, Room-Temperature Ferrimagnet with Frustrated Antiferroelectricity: Promising Candidate Toward Multiple-State Memory, Phys. Rev. X **4**, 011035 (2014).

[51] P. S. Wang, W. Ren, L. Bellaiche, and H. J. Xiang, Predicting a Ferrimagnetic Phase of Zn_2FeOsO_6 with Strong Magnetoelectric Coupling, Phys. Rev. Lett. **114**, 147204 (2015).

[52] J. C. Wojdeł and J. Íñiguez, *Ab initio* Indications for Giant Magnetoelectric Effects Driven by Structural Softness, Phys. Rev. Lett. **105**, 037208 (2010).